Available online at www.sciencedirect.com
ScienceDirect
Catalysis Today 129 (2007) 143–151
CATALYSIS TODAY
www.elsevier.com/locate/cattod

Quantum efficiency of cyanide photooxidation with TiO_2/SiO_2 catalysts: Multivariate analysis by experimental design

Javier Marugán [a], Rafael van Grieken [a,1], Alberto E. Cassano [b], Orlando M. Alfano [b,*]

[a] *Department of Chemical and Environmental Technology, ESCET, Universidad Rey Juan Carlos C/ Tulipán s/n, 28933 Móstoles, Madrid, Spain*
[b] *Instituto de Desarrollo Tecnológico para la Industria Química (INTEC), Universidad Nacional del Litoral-CONICET, Güemes 3450, 3000 Santa Fe, Argentina*

Available online 6 August 2007

Abstract

Despite the large amount of work dealing with supported photocatalysts used to overcome the difficulties associated with the recovery of powdered titania after the photocatalytic treatments, few attempts have been made to calculate the quantum efficiency (η) of these materials. In this work the quantum efficiency for the photooxidation of cyanide with TiO_2 and TiO_2/SiO_2 has been experimentally calculated using an approach based on the resolution of the radiative transfer equation inside the photoreactor. Due to the low absorption coefficient of the silica-supported material, a two-dimensional two-directional reactor model has been developed to describe the photon transport. The dependence of η on the incident radiation flux, the catalysts concentration and the cyanide concentration has been investigated. With both material suspensions, higher quantum efficiencies have been observed when lower radiation fluxes and higher cyanide concentrations are used. However, different trends in the quantum efficiencies are observed when increasing the catalyst concentration, leading to higher values when using powdered TiO_2 and lower values for TiO_2/SiO_2 suspensions.

Keywords: Photocatalysis; Photoreactor; Quantum efficiency; Supported TiO_2; Absorption; Scattering; Cyanide; Factorial design

1. Introduction

Heterogeneous photocatalytic processes have been the matter of research interest during the last two decades [1–5]. The application of this technology for the treatment of contaminated water has been shown to be environmental friendly, not only for being able of achieving the total mineralization of chemicals pollutants refractory to conventional treatments but also because of the possibility of using solar light to drive the process [6].

As one of the so-called advanced oxidation technologies, heterogeneous photocatalysis is based on the generation of highly reactive hydroxyl radicals that produce the unselective oxidation of organics chemicals. These species are formed upon irradiation of a semiconductor material, usually titanium dioxide, with photons of higher energy than the band gap of the material. The fundamentals of the process and the mechanism of degradation of a large number of pollutants have been extensively investigated [1–5]. However, the procedure for the correct comparison of the activity of different photocatalysts still remains a matter of discussion. There is an agreement that the primary parameter to assess the intrinsic activity of the material and the efficiency in the use of photons in a photocatalytic system is the ratio between the observed volumetric molar reaction rate of the process (r) and the volumetric rate of photon absorption by the semiconductor catalyst (e^a). This relation is called quantum yield (Φ_λ) or quantum efficiency (η) when using monochromatic or polychromatic radiation, respectively. Discrepancies arise in the experimental procedure to evaluate the value of e^a, due to the inherent difficulties derived from the simultaneous existence of absorption and scattering in heterogeneous systems. Several procedures have been reported in the literature [7–17] showing different degrees of experimental and theoretical complexities and certain advantages and disadvantages depending on the assumptions behind the applied radiation model.

One of the used approaches to evaluate the average volumetric rate of photon absorption inside the photoreactor

* Corresponding author. Tel.: +54 342 451 1546; fax: +54 342 451 1087.
E-mail addresses: rafael.vangrieken@urjc.es (R. van Grieken), alfano@intec.unl.edu.ar (O.M. Alfano).
[1] Tel.: +34 91 488 7007; fax: +34 91 488 7068.

0920-5861/$ – see front matter © 2007 Elsevier B.V. All rights reserved.
doi:10.1016/j.cattod.2007.06.060

is the rigorous solution of the radiation transfer equation (RTE). This equation provides the distribution of light intensities in the reaction space. The radiation field is required to calculate the kinetic model incorporated to the differential mass balance, when common chemical reactor engineering methods for the photoreactor design are followed [18].

Another point that has been the focus of many efforts is the development of supported photocatalysts, which improve the separation of the catalysts once the reaction is finished. The small size of the semiconductor particles commonly required to achieve high reaction rates in photocatalytic processes has been identified as one of the main drawbacks in the application of the photocatalytic technologies [19]. However, despite the large number of supported TiO_2 photocatalysts reported in the last years, not many attempts have been made to estimate quantum efficiencies for this kind of materials.

This work deals with the determination of the absolute quantum efficiency for free cyanide photooxidation using a silica-supported TiO_2 photocatalyst and the comparison with the results obtained with powder titania suspensions. The influence of initial concentration of cyanide, catalysts concentration and incident photon flux has been studied by using a statistical approach based on a design of experiments that allows performing the minimum number of experiments with the simultaneous determination of the interaction between variables.

2. Experimental

2.1. Catalysts

The TiO_2/SiO_2 photocatalyst with a nominal content of 40 wt% of TiO_2 was synthesized by incorporating titania into a silica support (INEOS Silica ES70Y, 257 $m^2\ g^{-1}$ of specific surface area) through a sol–gel method. This catalyst will be named as 40% TiO_2/SiO_2. It consists of titanium dioxide nanocrystals with an average size of 7.2 nm homogeneously distributed over the surface of the silica particles. Aldrich TiO_2 (>99% anatase, 7.1 $m^2\ g^{-1}$ of specific surface area) has been used as reference material to compare the results. More details about the characterization and optical properties of both materials can be found elsewhere [20].

2.2. Photoreactor

The experimental setup for the photocatalytic reactions consists of a cylindrical reactor 6 cm long and 5 cm in diameter made of borosilicate glass with two circular flat windows and two ports for the entrance and exit of the reactant and products solution. The radiation enters the reactor through one of the windows, which has been externally treated with HF to produce a ground glass texture. This feature is very important, as it allows the assumption of a diffuse incoming radiation in the boundary condition of the radiation transport equation applied to the photoreactor. The photoreactor is part of a recycling system operating in closed circuit with a stirred reservoir tank of 2 L volume equipped with a sample system and a recirculating pump (Fig. 1).

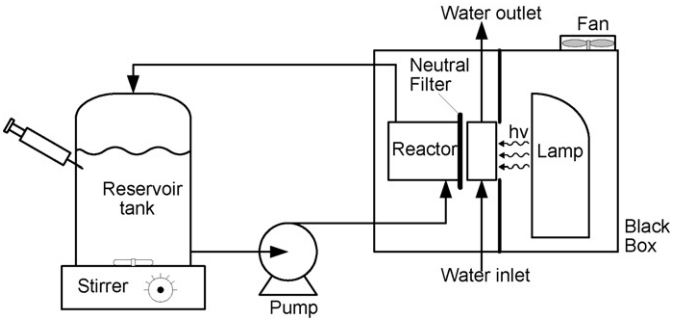

Fig. 1. Schematic representation of the experimental setup.

Illumination was carried out using a Osram Ultramed 400W lamp that provides a nominal UV-A irradiation power of 82 W. Radiation enters the reactor chamber crossing a water-cooled filter that absorbs the infrared radiation, avoiding the overheating of the suspension. Reactor and lamp are placed inside a black box to avoid uncontrolled inlet radiation and to prevent hurting of the operator from UV irradiation. For the first reason, pipes and tank are also covered.

The radiation flux entering the reactor was controlled using home-made neutral filters placed in front of the inlet window. Filters were prepared by high-quality laser printing of controlled black coverage levels onto a transparent substrate using CorelDraw® software. Reproducibility of the preparation procedure and stability of the filters along several hours of irradiation was checked by measuring the transmission spectra with a Varian Cary 500 Scan UV–vis–NIR spectrophotometer and the filtered UV radiation flux using a Gigahertz-Optik X97 irradiance meter. Quantitative values of the radiation flux entering the reactor were experimentally determined by ferrioxalate actinometry [21].

The wavelength relative distribution of the incident radiation was measured using a CVI Hand-held SM240 CCD spectrometer, which agrees with the emission spectrum of the lamp reported by the manufacturer.

2.3. Reactions

Cyanide photooxidation experiments were carried out at a temperature of 25 ± 2 °C and pH value of 12. Deionized water (Milli-Q®, 18.2 MΩ cm) was used to prepare the solutions of potassium cyanide (Panreac, reagent grade) and the pH was adjusted with sodium hydroxide (Scharlab, reagent grade). The required amount of catalyst was added and the suspension was stirred and saturated with molecular oxygen by bubbling for 30 min. In the meantime, the lamp was switched on to stabilize its emission power and spectrum.

During the reaction, which usually lasted for 1 h, samples were taken every 10 min from the reservoir tank and filtered through 0.22 μm nylon membranes to remove the catalyst before analysis. Temperature and pH measurements were performed to check that both parameters remained essentially constant. Removal of CN^- was followed by the pyridine-barbituric standard colorimetric method [22]. Although the method is very sensitive and reproducible, four different measurements were conducted on every sample to quantify the

experimental error and increase the statistical significance of the experimental results obtained when operating with low cyanide conversion conditions.

3. Results and discussion

3.1. Photon absorption

As it has been mentioned previously, for the estimation of the average volumetric rate of photon absorption, the photon transport inside the reactor must be modelled and the radiation field has to be calculated by solving the radiative transfer equation (RTE) [18]. The solution of the model requires of two sequential steps: (i) the evaluation of the inlet radiation flux as a function of the irradiation rates by means of ferrioxalate actinometry and (ii) the calculation of the average volumetric rate of photon absorption inside the reactor as a function of the catalyst concentration. This can be done when the absorption and scattering coefficients and the scattering phase function of the suspension are known.

3.1.1. Inlet radiation

Filters with increasing black coverage were prepared according to the procedure described in the experimental section. A linear dependence was found in the range between 10 and 90% of black coverage of the filter. Transmission spectra of the filters in the UV-A wavelength range were recorded and used to correct the emission spectrum of the lamp.

Values of the radiation flux entering the reactor were experimentally calculated by applying the mass balance of the reactor to the ferrioxalate actinometry runs. Assuming that (i) the system is perfectly mixed, (ii) there are no mass transport limitations, (iii) the conversion per pass in the reactor is differential and (iv) there are no parallel dark reactions, the Fe(II) mass balance could be expressed as follows [23]:

$$\varepsilon_L \left.\frac{dC_{Fe(II)}(t)}{dt}\right|_{Tk} = \frac{V_R}{V_T}\left\langle r_{Fe(II)}(x,t)\right\rangle_{V_R} \quad (1)$$

where ε_L is the liquid hold-up ($\varepsilon_L = 1$ for a homogeneous system), $C_{Fe(II)}$ the molar concentration of Fe(II), t denotes reaction time, Tk, R and T subindexes refer to the tank, reactor and total, respectively, and $\langle r_{Fe(II)}(x,t)\rangle V_R$ is the Fe(II) formation reaction rate averaged over the reactor volume.

The procedure to calculate the incoming radiation flux consists of the following steps:

(i) For every experimental run, the $\lim_{t\to 0} dC_{Fe(II)}(t)dt|_{Tk}$ was calculated from the lineal plot of the Fe(II) concentration measured in the tank versus time.

(ii) The expression of the reaction rate of Fe(II) formation can be derived from Eq. (1):

$$\left\langle r_{Fe(II)}(x,t)\right\rangle_{V_R} = \frac{V_T}{V_R}\lim_{t\to 0}\left.\frac{dC_{Fe(II)}(t)}{dt}\right|_{Tk} \quad (2)$$

(iii) Assuming the value of $\phi_{366\ nm} = 1.21$ [21] as the average quantum yield for the whole studied wavelength range $\langle\phi\rangle_\lambda$ and knowing the area of the radiation inlet window, S_R^{irr}, the photon flux entering the reactor can be calculated as follows:

$$q^0 = \left\langle r_{Fe(II)}(x,t)\right\rangle_{V_R}\frac{V_R}{\left\langle\phi\right\rangle_\lambda S_R^{irr}} \quad (3)$$

In Eq. (3), a sufficiently high actinometer concentration and a complete absorption of the emitted photons by the lamp entering into the reactor for all the existing wavelengths have been assumed.

The value of q^0 corresponds to the incoming radiation in the whole absorption wavelength spectrum of the potassium ferrioxalate actinometer. The wavelength discretization of the incident photon flux, q_λ^0, was performed according to: (i) the relative intensities of the lamp emission spectrum measured with a spectrophotometer, (ii) the spectral transmission of every filter and (iii) the normalizing condition, $q^0 = \int_\lambda q_\lambda^0\, d\lambda$, in the studied wavelength range delimited for the transmission of the filters and the window glass (~320 nm) and the absorption of the actinometer and lamp emission (~400 nm). Assuming that the ground glass of the reactor window produces a diffuse radiation, the values of the directional intensities entering the reactor can be calculated as $I_\lambda^0 = q_\lambda^0/\pi$.

3.1.2. Average volumetric rate of photon absorption

The spectral distribution of the incident radiation calculated in the previous section constitutes the experimental boundary condition required for the determination of the volumetric rate of photon absorption inside the reactor. The other essential information that needs to be experimentally obtained is the spectral distribution of the optical properties of the catalyst suspension, that are the absorption and scattering coefficients and the phase function. Fig. 2 depicts the relative spectral distributions of the absorption coefficients of both photocatalysts in comparison with the spectral distribution of the radiation entering the reactor. The maximum emission of the lamp is located in a wavelength range in which the relative absorption of the catalysts is very low. In contrast, the maximum absorption of both materials takes place at wavelengths where the emission of the lamp is not so high. Additionally, although both materials absorb radiation below 390 nm, their relative absorption spectra are slightly different. As the wavelength decreases, the absorption of Aldrich TiO_2 first increases and then reaches a plateau, whereas the absorption of 40% TiO_2/SiO_2 is always crescent, being lower than that of Aldrich TiO_2 at higher wavelengths and higher at lower values of λ. Consequently, it is very important to remark that the wavelength discretization of the radiative properties is always required for the rigorous evaluation of the photon absorption rate. The absolute values of the absorption and scattering coefficients and the scattering phase functions of both catalysts, and the procedure for their calculation can be found elsewhere [20,24].

For the estimation of the average volumetric rate of photon absorption, the radiative transfer equation (RTE) that describes the transport of photons inside the reactor must be solved [25]. Assuming that the emission of radiation could be considered

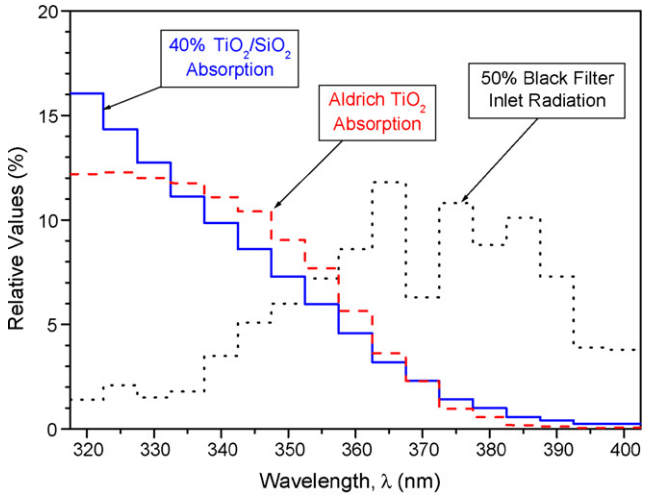

Fig. 2. Relative spectral distribution of the absorption coefficients of Aldrich TiO_2 and 40% TiO_2/SiO_2 materials in comparison with the spectral distribution of the inlet radiation.

negligible at the low working temperatures of the photocatalytic processes, and that the steady state condition could be applied, *e.g.*, the optical properties of the suspension do not change with time, the RTE takes the following expression:

$$\frac{\mathrm{d}I_{\lambda,\underline{\Omega}}(\underline{x})}{\mathrm{d}s} = -\underbrace{\kappa_\lambda(\underline{x})I_{\lambda,\underline{\Omega}}(\underline{x})}_{\text{absorption}} - \underbrace{\sigma_\lambda(\underline{x})I_{\lambda,\underline{\Omega}}(\underline{x})}_{\text{out-scattering}} + \underbrace{\frac{\sigma_\lambda(\underline{x})}{4\pi}\int_{\Omega'=4\pi} p(\underline{\Omega}'\rightarrow\underline{\Omega})I_{\lambda,\underline{\Omega}'}(\underline{x})\,\mathrm{d}\Omega'}_{\text{in-scattering source term}} \quad (4)$$

The solution of this integro-differential equation provides the radiation field inside the photoreactor, that is the value of the intensity of photons of the monochromatic radiation for each direction of the spherical space and for each differential elementary volume of the reactor, $I_{\lambda,\underline{\Omega}}(\underline{x})$. Once the intensities are known, the monochromatic local volumetric rate of photon absorption (LVRPA) can be obtained by calculating the incident radiation through the integration of the whole spherical space of directions and multiplying by the volumetric absorption coefficient:

$$\mathrm{LVRPA} = e^{\mathrm{a}}_{\lambda} = \kappa_\lambda(\underline{x})G_\lambda(\underline{x}) = \kappa_\lambda(\underline{x})\int_{\Omega=4\pi} I_{\lambda,\underline{\Omega}}(\underline{x})\,\mathrm{d}\Omega \quad (5)$$

The rigorous numerical resolution of the radiation propagation in multidimensional systems could be achieved by two main groups of procedures: (i) probabilistic models, especially Monte Carlo simulations [13,15,16,26,27] and (ii) discretization methods for the integration of the RTE, from which the discrete ordinate method (DOM) has shown a wide range of applications with no restrictions about the geometry or the anisotropy of the system [11,14,18,20,28,29]. The DOM, initially developed in the field of nuclear engineering to describe the neutron transport, transforms the integro-differential expression of the RTE into a system of finite differences algebraic equations that can be solved by numerical computation [30].

In a previous work, Brandi et al. [14] applied a one-dimensional one-directional model to describe the transport of the photons inside a reactor very similar to that used in this work. The assumption of this model was justified by the two different features: (i) the dimensions of the reactor were high enough to assume that a total absorption of photons is produced and no radiation exits through the lateral wall of the cylinder and (ii) the existence of azimuthal symmetry based on the boundary condition of diffuse incoming radiation achieved with the ground glass window. The latter condition could be also applied in the present system. However, due to the low absorption coefficients of the TiO_2/SiO_2 photocatalyst [20], the assumption of null outgoing photon flux through the lateral wall of the reactor would be a poor approximation. For this reason, a cylindrical two-dimensional (r, z) two-directional (θ, ϕ) model of the photoreactor had to be developed. Fig. 3 shows the Gaussian quadrature scheme used for the discretization of the spherical space of directions as a function of the direction cosines (μ, η) and the spatial mesh defined for the 2D discretization of the cylindrical reactor.

As shown by Duderstadt and Martin [30], for multi-dimensional geometries it is recommended to derive the finite difference relations directly from the radiation balance for each mesh cell, rather than introducing the finite difference approximation directly into the RTE. Fig. 3c (left) schematizes the cross section of the spatial cell. The basic idea behind the DOM is to generate a system of equations in such way that it can be used to solving the photon transport equation following the direction of propagation. For instance, Fig. 3c (right) shows the resolution of the photon transport for directions of quadrant II. This set of directions is solved by calculating the intensity in the center of the cell from the inlet radiation fluxes coming through the upper and right surfaces of the cell and also calculating the outgoing radiation fluxes through the left and bottom surfaces of it. As it can be observed, the inlet and outlet surfaces depend on the quadrant of the considered direction of propagation. The balance of photons with a given wavelength λ propagated through the cell along the direction Ω_m can be found elsewhere [30].

The system of algebraic equations to be solved is constituted by the application of the balance of photons with a given wavelength λ to each cell of the spatial and directional meshes, together with the following boundary conditions:

(i) Null reflection on the cylindrical wall at $r = L_R$ (quadrants II and III).
(ii) Known inlet radiation at $z = 0$ (quadrants I and II).
(iii) Null reflection on the wall at $z = L_Z$ (quadrants III and IV).
and the symmetry condition in the axis of the cylinder:
(iv) At $r = 0$ quadrants I and IV are symmetric to quadrants II and III, respectively.

The algorithm developed to solve the system of equations begins the computations from the corner of the spatial mesh in which two of the four conditions can be applied. First, the central intensity is obtained from the inlet values, and then the

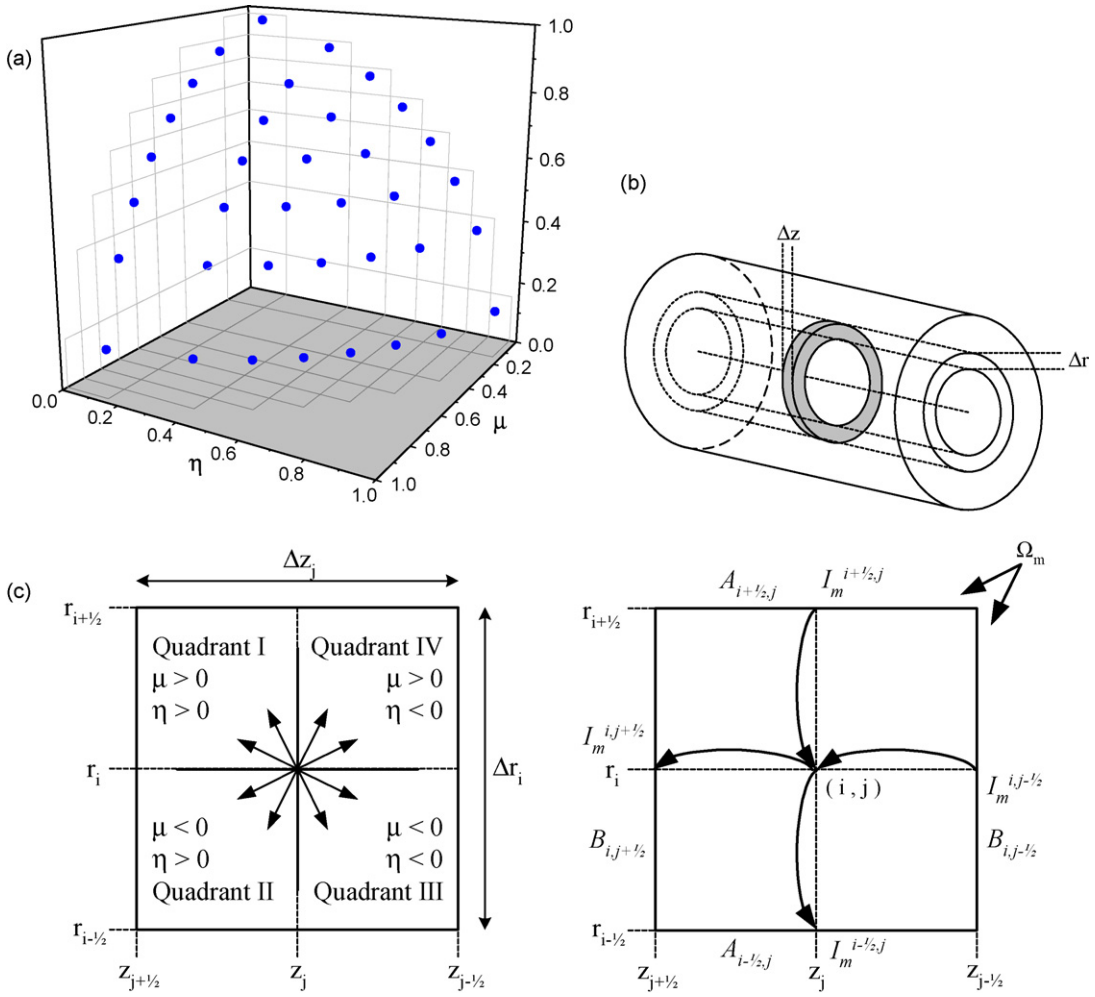

Fig. 3. (a) Directional mesh and (b) spatial mesh for the two-directional two-dimensional discretization of the photoreactor. (c) Cross section of the spatial cell. Definition of the quadrants of directions as a function of the direction cosines (μ, η) respect to z- and r-axis, respectively (left), and example of the calculus of the intensity in the central point and outlet surfaces of the cell from the intensities of radiation entering trough the inlet surfaces (right).

outlet intensities are readily calculated. Convergence of the radiation field is achieved when the intensities initially employed for the calculus of the in-scattering terms coincide with the calculated values.

Fig. 4(a) displays the profile of the net radiation flux along the axial coordinate of the photoreactor for increasing concentrations of the two studied materials. The decrease in the photon concentration is more pronounced when using Aldrich TiO_2 than with a higher concentration of TiO_2 supported on silica. However, the differences between powdered and supported titania are more marked when the average e^a is calculated. Fig. 4(b) shows the dependence of the average volumetric rate of photon absorption on the catalyst concentrations of the suspension. Whereas Aldrich TiO_2 reach the maximum value of $\langle e^a \rangle$ near a concentration of 0.2 g L^{-1}, the 40% TiO_2/SiO_2 suspensions absorb far less photons employing similar concentrations of titania. However, they reach values close to those of Aldrich TiO_2 when the catalysts concentration is sufficiently increased.

The spectral distribution of the volumetric photon absorption is represented in Fig. 4c. As expected, in both cases the higher values are obtained in the range from 340 to 375 nm, in which the maximum overlapping of the lamp emission and catalyst absorption spectra is produced.

3.2. Quantum efficiencies for cyanide photoxidation

Once the volumetric rates of photon absorption were estimated, the photocatalytic reactions for cyanide oxidation were planned according to a two-level factorial design in the following experimental domain:

- *F1*: Catalyst concentration, C_{cat} (g L^{-1}): 0.1 (−1)/0.3 (+1) for Aldrich TiO_2 and 1.0 (−1)/3.0 (+1) for 40% TiO_2/SiO_2.
- *F2*: CN^- concentration, $C_{CN}-$ (mg L^{-1}): 15.0 (−1)/45.0 (+1)
- *F3*: Incident photon flux, q^0 ($\times 10^4$ einstein m^{-2} s^{-1}): 5.86 (−1)/20.0 (+1).

The incident photon fluxes correspond to the filters with 70 and 30% black coverage, whereas the catalysts concentrations range have been selected to get similar values of the volumetric rate of photon absorption. Additionally, two experiments were

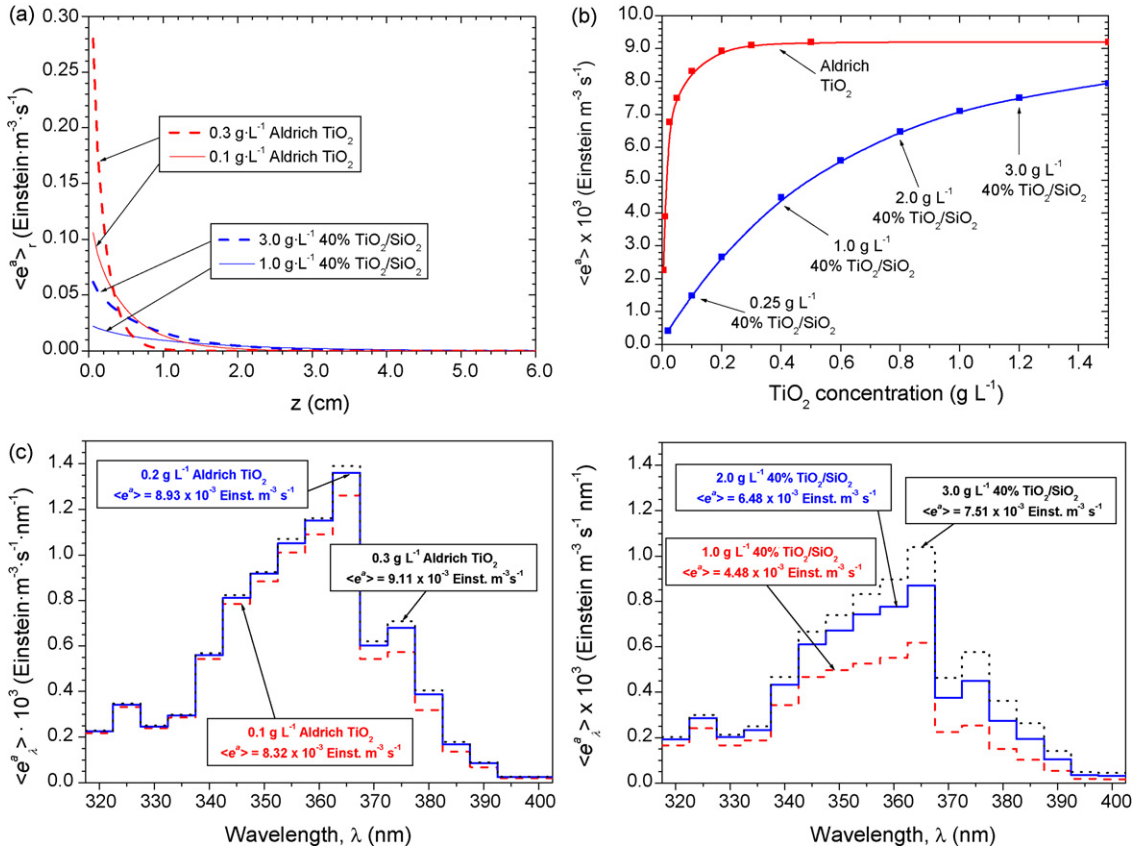

Fig. 4. Comparison of the *r*-averaged LVRPA axial profiles (a) and dependence of the average LVRPA on the titanium dioxide concentration (b) for Aldrich TiO_2 and 40% TiO_2/SiO_2 materials using the 50% neutral filter. (c) Spectral distribution of the LVRPA for different concentrations of Aldrich TiO_2 (left) and 40% TiO_2/SiO_2 (right) using the 50% neutral filter.

carried out to compare the activity of both materials using equal concentrations of titanium dioxide.

The experimental design consisted of eight experiments carried out in the different combinations of the minimum and maximum values of the three variables plus four different replicates of the central point to evaluate both the experimental error and the possible existence of a non-linear dependence of the response variable to the initial reaction rate of cyanide photooxidation. Fig. 5 shows the cyanide concentration profiles observed in three different experiments for every catalyst: (i) the central point of the design, codified as (0 0 0), (ii) the experiment in which the maximum reaction rate is expected (+1,+1,+1) and (iii) that one in which the minimum value should be obtained (−1,−1,−1).

As it can be seen, in all cases the conversion is small enough to consider that: (i) the amount of formed products is negligible, (ii) the stoichiometric consumption of oxygen is low and the dissolved oxygen could be considered constant and (iii) the change in cyanide concentration is low and could be assumed that it does not affect the reaction rate. Consequently, initial conditions can be supposed during the whole reaction and the results can be fitted to a straight line to calculate the slope. However, such a low cyanide conversion means a relatively high analytical error. For that reason four replicates of the cyanide quantification of every sample were carried out, being the error bars of Fig. 5 the standard deviation of the results.

Following a similar procedure to that shown for the ferrioxalate actinometry runs, the initial reaction rate of cyanide photooxidation can be derived from the slope of the plot of the cyanide concentration in the tank versus time by applying the mass balance of the reactor as follows:

$$\left\langle r^0_{CN^-}(x,t)\right\rangle_{V_R} = \frac{V_T}{V_R}\lim_{t\to 0}\frac{dC_{CN^-}(t)}{dt}\bigg|_{Tk} \tag{6}$$

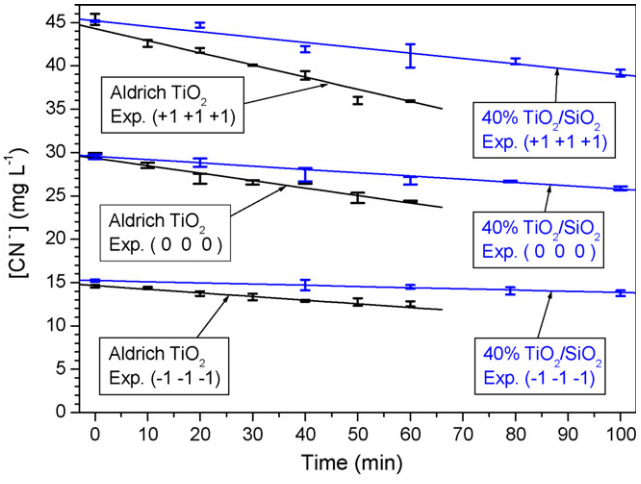

Fig. 5. Cyanide concentration profiles of selected experiments.

Table 1
Experimental results of the cyanide photooxidation rate, calculated values for the average volumetric rates of photon absorption and quantum efficiencies

Experiment	$\langle r^0_{CN^-} \rangle_{V_R}$ ($\times 10^5$ mol_{CN} m^{-3} s^{-1})		$\langle e^a \rangle_{V_R}$ ($\times 10^3$ einstein m^{-3} s^{-1})		η_{CN} (%)	
	Aldrich TiO_2	40% TiO_2/SiO_2	Aldrich TiO_2	40% TiO_2/SiO_2	Aldrich TiO_2	40% TiO_2/SiO_2
−1 −1 −1	18.1	6.86	3.75	2.02	4.8	3.4
+1 −1 −1	24.5	13.3	4.11	3.39	6.0	3.9
−1 +1 −1	28.4	11.4	3.75	2.02	7.6	5.6
+1 +1 −1	36.5	15.3	4.11	3.39	8.9	4.5
−1 −1 + 1	44.2	16.1	12.8	6.91	3.5	2.3
+1 −1 +1	56.5	21.0	14.0	11.6	4.0	1.8
−1 +1 +1	75.1	21.3	12.8	6.91	5.9	3.1
+1 +1 +1	92.5	28.8	14.0	11.6	6.6	2.5
0 0 0	48.9	21.0	8.93	6.48	5.5	3.2
0 0 0	54.3	20.0	8.93	6.48	6.1	3.1
0 0 0	45.5	17.0	8.93	6.48	5.1	2.6
0 0 0	46.7	20.0	8.93	6.48	5.2	3.1
0.1 g_{Tio_2} L^{-1}, 30 mg_{CN} L^{-1}, filter 50%	43.7	9.10	8.32	1.49	5.3	6.1

Table 1 summarizes the results obtained for the cyanide photooxidation rates together with the average volumetric rates of photon absorption and the quantum efficiencies, calculated according to

$$\eta_{CN} = \frac{\left\langle r^0_{CN} \right\rangle_{V_R}}{\left\langle e^a \right\rangle_{V_R}} \tag{7}$$

Experiments are named according to the codified levels of the variables. Although they have been sorted to be shown in a more intuitive way, they were carried out following a random sequence to avoid systematic errors.

A statistical approach has been used to model the dependence of the quantum efficiency with the three studied variables. The curvature of the response, that is the difference between the average of the eight experiments of the factorial design and the average of the central point replicates, was found to be below its corresponding error. Consequently, there is no need to perform additional experiments, and the results can be successfully fitted using linear models whose parameters are calculated using a least-squares multiple linear regression algorithm. Additionally, the application of the Yates's algorithm shows that in both cases the effects corresponding to most of the binary and ternary interactions among the variables are below the experimental error. Therefore, only the linear terms of the three variables and the interaction between catalyst concentration and cyanide concentration for the 40% TiO_2/SiO_2 catalyst are considered significant. More details of the statistical procedures for data treatment and the calculus of the errors can be found elsewhere [31]. The obtained equations are:

$$\eta_{CN}\,(\%) = 3.89 + 4.74C_{cat} + 0.089C_{CN^-} - 0.128q^0, \quad \text{error} = \pm 0.28 \tag{8}$$

for Aldrich TiO_2, and:

$$\eta_{CN}\,(\%) = 3.65 + 0.212C_{cat} + 0.064C_{CN^-} - 0.138q^0 - 0.0143C_{cat}C_{CN^-}, \quad \text{error} = \pm 0.42 \tag{9}$$

for the catalyst 40% TiO_2/SiO_2.

The existence of a significant interaction between the catalyst and cyanide concentrations could be related with the contribution of internal transport inside the porous structure of the supported catalysts in the observed reaction rate, but this hypothesis would need further experiments and theoretical modeling to be verified.

The three-dimensional plots of both response surfaces at constant cyanide concentration are displayed in Fig. 6, together with the experimental points to show the fitting goodness.

In both cases, higher values of η_{CN} are achieved at lower incident photon fluxes, in agreement with the results previously reported for the photooxidation of 4-chlorophenol [32]. Both materials also show higher quantum efficiencies when increasing the cyanide concentration; consequently, this becomes the most influencing variable. However, there is an important difference in the dependence with the catalyst concentration of both materials. For Aldrich TiO_2, an increase in the loading of the suspension leads to higher quantum efficiencies in all the studied range of incident photon fluxes and cyanide concentrations. In contrast, when 40% TiO_2/SiO_2 is used as photocatalyst, η remains almost unaffected or even decreases with the increase in catalyst concentration. Notice for example the experimental results corresponding to the code levels (−1,+1,−1) and (+1,+1,−1), shown in Table 1, rows 3 and 4. For the Aldrich TiO_2 catalyst, an increase of 9.6% of the $\langle e^a \rangle_{V_R}$ (from 3.75×10^{-3} to 4.11×10^{-3} einstein m^{-3} s^{-1}) yields an increase of 28% of the $\langle r^0_{CN^-} \rangle_{V_R}$ (from 28.4×10^{-5} to 36.5×10^{-5} mol_{CN} m^{-3} s^{-1}). A similar comparison for the 40% TiO_2/SiO_2 catalyst, gives the following results: an increase of 68% of the $\langle e^a \rangle_{V_R}$ (from 2.02×10^{-3} to 3.39×10^{-3} einstein m^{-3} s^{-1}) produces an increase of only 34% of the $\langle r^0_{CN^-} \rangle_{V_R}$

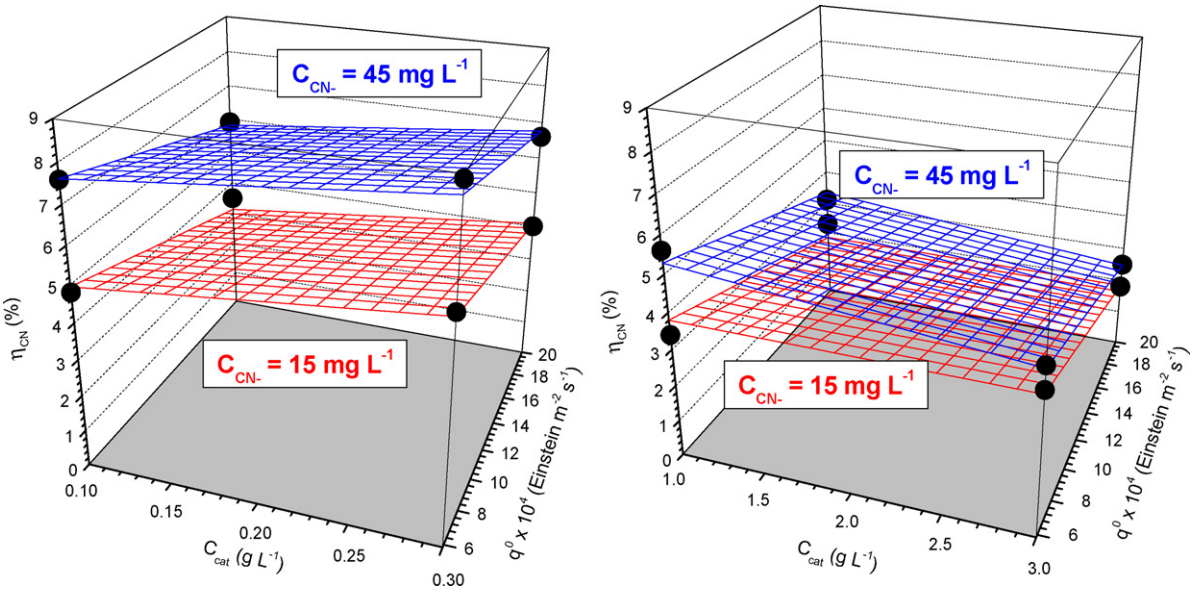

Fig. 6. 3D graphical representation of the quantum efficiency response surfaces at constant cyanide concentration with Aldrich TiO_2 (left) and 40% TiO_2/SiO_2 (right). (●) represents the experimental points.

(from 11.4×10^{-5} to 15.3×10^{-5} $mol_{CN}\ m^{-3}\ s^{-1}$). Clearly, for the supported TiO_2 catalyst, a much higher increase of the average volumetric rate of photon absorption (68%) is necessary to get a similar increase of the cyanide photooxidation rate (34%). Consequently, an increase in the catalyst loading leads to a higher quantum efficiency for Aldrich TiO_2 (from 7.6 to 8.9) and a lower quantum efficiency for the 40% TiO_2/SiO_2 (from 5.6 to 4.5).

The explanation for this different behavior is not so obvious to find. First of all, it must be noticed that the quantum efficiency is not dependent directly on the incident photon flux but on the volumetric rate of photon absorption. Of course, as the radiation entering the reactor increases higher values of e^a are achieved, but they are strongly dependent on the absorption properties of the suspensions. As the supported photocatalyst shows lower absorption coefficients, the values of the quantum efficiencies are more influenced by the calculated values of e^a, as it can be drawn from the reported results. In fact, when comparing the activity of both materials at equal titanium dioxide concentrations (additional experiment in Table 1) surprising results are obtained. In spite of the fact that the observed reaction rate of 40% TiO_2/SiO_2 suspension is almost five times smaller than that shown by Aldrich TiO_2, the calculated quantum efficiency is higher, as a consequence of the low volumetric rate of photon absorption.

Concerning the results shown in Fig. 6 (right), it should be noted that the SiO_2-supported photocatalyst is constituted by large silica particles of 50–70 μm with small TiO_2 crystals of ca. 7 nm homogeneously distributed on the porous structure. The silica material is transparent to the UV radiation (this is one of the premises to be used as support) and theoretically all the titania nanocrystals inside the particles could be illuminated. On the other hand, the cyanide molecules need to diffuse inside the porous structure of the catalyst. Let us consider two different situations. First, a high catalyst concentration is used; it leads to a high volumetric rate of photon absorption and a pronounced radiation profile according to the results displayed in Fig. 4. Second, a low catalyst concentration is used: it produces a lower value of e^a and a slower decrease of the radiation flux along the reactor. In the first situation most of the absorption is produced in the reactor volume close to the radiation entrance window, whereas in the second one, the reaction takes place in the whole reactor volume. Considering that there are no limitations to the photon transport inside the particles, but there are limitations to the internal mass transport of cyanide, the first system should show a higher amount of photons absorbed by the TiO_2 nanocrystals in the most inner part of the silica particles that are not efficient in successfully oxidizing cyanide because of internal diffusion control of the reactant and thus increasing the recombination rate of electrons and holes. This internal mass transfer limitation inside the catalytic particle explains why the quantum efficiency remains almost constant or decreases when the concentration of the 40% TiO_2/SiO_2 catalyst is increased (Fig. 6, right).

4. Conclusions

The quantum efficiency for the photooxidation of cyanide with TiO_2 and TiO_2/SiO_2 materials has been calculated by solving the radiation transfer equation inside the experimental photoreactor. The influence of the incident photon flux, catalyst concentration and cyanide concentration has been determined. In both catalytic systems higher efficiencies have been observed when lower radiation fluxes and higher cyanide concentrations are used. However, different trends are observed when increasing the catalyst concentration, leading to higher values when using powdered TiO_2 and lower values for TiO_2/SiO_2 suspensions. This apparently anomalous result has been explained by the existence of internal mass

transfer limitations inside the TiO_2/SiO_2 porous structure. The axial distribution of the local volumetric rate of photon absorption for high catalyst concentrations has been used to explain these results. For this case, the high amount of photons absorbed by the TiO_2 nanocrystals near the radiation entrance window is not useful for the photocatalytic reaction because of internal catalytic particles transport limitations of the cyanide molecules. On the contrary, for low catalyst concentrations of TiO_2/SiO_2, the local volumetric rate of photon absorption presents a slower decrease along the axial coordinate and the effect of internal mass transfer limitations is not important.

The quantum efficiency of the 40% TiO_2/SiO_2 photocatalyst is higher than the one obtained with powdered TiO_2 when using equal mass of titania as a consequence of the lower absorption coefficients of the supported materials. However, a higher efficiency is achieved with powdered titania when similar volumetric rates of photon absorption are compared.

Acknowledgments

Financial support from the Spanish Ministerio de Ciencia y Tecnología through the program Consolider-Ingenio 2010 (project CSD2006-00044 TRAGUA), Comunidad de Madrid through the program REMTAVARES S-0505/AMB/0395 and from the Universidad Nacional del Litoral, Agencia Nacional de Promoción Científica y Tecnológica, and Consejo Nacional de Investigaciones Científicas y Técnicas (Argentina) are gratefully acknowledged. O.M. Alfano also thanks Agencia Española de Cooperación Internacional (AECI) and Universidad Rey Juan Carlos for the financial support of his stay in Móstoles (Madrid, Spain) through the ''Programa de Cooperación Interuniversitaria'' (PCI-C/2876/05).

References

[1] M. Schiavello (Ed.), Photocatalysis and Environment. Trends and Applications, Wiley, New York, 1989.
[2] D.F. Ollis, H. Al-Ekabi (Eds.), Photocatalytic Purification and Treatment of Water and Air, Elsevier, Amsterdam, 1993.
[3] D. Blake, Bibliography of work on the photocatalytic removal of hazardous compounds from water and air, NREL Golden Co., (May 1994; 1st update: October 1994; 2nd update: October 1996; 3rd update: January 4th update: October 2001), 1999
[4] M.R. Hoffmann, S.T. Martin, W. Choi, D.W. Bahnemann, Chem. Rev. 95 (1995) 69.
[5] J.M. Herrmann, Catal. Today 53 (1999) 115.
[6] I. Muñoz, J. Rieradevall, F. Torrades, J. Peral, X. Doménech, Sol. Energy 79 (2005) 369.
[7] L. Palmisano, V. Augugliaro, R. Campostrini, M. Schiavello, J. Catal. 143 (1993) 149.
[8] L. Sun, J.R. Bolton, J. Phys. Chem. 100 (1996) 4127.
[9] N. Serpone, J. Photochem. Photobiol. A: Chem. 104 (1997) 1.
[10] U. Stafford, K.A. Gray, P.V. Kamat, J. Catal. 167 (1997) 25.
[11] M.I. Cabrera, O.M. Alfano, A.E. Cassano, J. Adv. Oxid. Technol. 3 (1998) 220.
[12] M. Salaices, B. Serrano, H.I. de Lasa, Ind. Eng. Chem. Res. 40 (2001) 5455.
[13] D. Curcó, J. Giménez, A. Addardak, S. Cervera-March, S. Esplugas, Catal. Today 76 (2002) 177.
[14] R.J. Brandi, M.A. Citroni, O.M. Alfano, A.E. Cassano, Chem. Eng. Sci. 58 (2003) 979.
[15] T. Yokota, S. Cesur, H. Suzuki, H. Baba, Y. Takahata, J. Chem. Eng. Jpn. 32 (1999) 314.
[16] Q. Yang, P.L. Ang, M.B. Ray, S.O. Phekonen, Chem. Eng. Sci. 60 (2005) 5255.
[17] V. Loddo, M. Addamo, V. Augugliaro, L. Palmisano, M. Schiavello, AIChE J. 52 (2006) 2565.
[18] A.E. Cassano, O.M. Alfano, Catal. Today 58 (2000) 167.
[19] R.L. Pozzo, M.A. Baltanás, A.E. Cassano, Catal. Today 39 (1997) 219.
[20] J. Marugán, R. van Grieken, O.M. Alfano, A.E. Cassano, AIChE J. 52 (2006) 2832.
[21] A.M. Braun, M.T. Maurette, E. Oliveros, Photochemical Technology, Wiley, Chichester, 1991.
[22] L.S. Clescerl, A.E. Greenberg, A.D. Eaton (Eds.), Standard Methods for the Examination of Water and Wastewater, United Book Press Inc., Baltimore, MD, USA, 1998.
[23] M.I. Cabrera, A. Negro, O.M. Alfano, A.E. Cassano, J. Catal. 172 (1997) 380.
[24] M.L. Satuf, R.J. Brandi, A.E. Cassano, O.M. Alfano, Ind. Eng. Chem. Res. 44 (2005) 6643.
[25] M.N. Ozisik, Radiative Transfer and Interactions with Conduction and Convection, Wiley, New York, 1973.
[26] M. Pasquali, F. Santarelli, J.F. Porter, P.L. Yue, AIChE J. 42 (1996) 532.
[27] C.A. Arancibia-Bulnes, J.C. Ruiz-Suarez, Appl. Optics 38 (1999) 1877.
[28] G. Slagari, G. Camera-Roda, F. Santarelli, Int. Commun. Heat Mass Transfer 5 (1998) 651.
[29] L.R. Romero, O.M. Alfano, A.E. Cassano, Ind. Eng. Chem. Res. 36 (1997) 3094.
[30] J.J. Duderstadt, W.R. Martin, Transport Theory, Wiley, New York, 1979.
[31] G.E.P. Box, W.G. Hunter, J.S. Hunter, Statistics for Experimenters: An Introduction to Design, Data Analysis and Model Building, Wiley, New York, 1978.
[32] M.L. Satuf, R.J. Brandi, A.E. Cassano, O.M. Alfano, Ind. Eng. Chem. Res. 46 (2007) 43.